Lymphology 57 (2024) 132-141

THE ADDED EFFECT OF ARTIFICIAL INTELLIGENCE IN CT ASSESSMENT OF ABDOMINAL LYMPHADENOPATHY

R.A. Meshref, I.A. Saleem, A.A. Salama, S.H. Darwish, S.M. El-Kholy, E.I. Mohamed

Medical Equipment Technology Department, Faculty of Applied Health Sciences Technology, Pharos University, Alexandria, Egypt (RAM); Medical Biophysics Department, Medical Research Institute, Alexandria University, Alexandria, Egypt (IAS, SMK, EIM); Optometry Department, Technical Medical Institute, Erbil Polytechnic University, Erbil, Iraq (IAS); Research and Development Center, Air Defense College, Alexandria; Egypt (AAS); and Higher Institute of Engineering and Technology – King Mariout, Alexandria, Egypt (SHD)

ABSTRACT

Lymphadenopathy is associated with lymph node abnormal size or consistency due to many causes. We employed the deep convolutional neural network ResNet-34 to detect and classify CT images from patients with abdominal lymphadenopathy and healthy controls. We created a single database containing 1400 source CT images for patients with abdominal lymphadenopathy (n = 700) and healthy controls (n = 700). To train, test, and cross-validate the ResNet-34 classifier to detect specific lesions, we first resized and normalized all images. Then, we randomly divided the 1400 images into 88 groups of 16, and the classifier was trained to identify and label lesions using automatic volume delineation 3D reconstruction of target areas. The ResNet-34 had a diagnostic accuracy with receiver operating characteristic (ROC) curves of the true-positive rate versus the false-positive rate with the area under the curve (AUC) of 0.9957 and 1.00 for abdominal lymphadenopathy and healthy control CT images, respectively. This accuracy implied identical high sensitivity and specificity values of 99.57 % and 100% for the two groups. The added effect of ResNet-34 is a success rate of 99.57% and 100% for classifying random CT images of the two groups, with an overall accuracy of 99.79% in the testing subset for detecting and classifying lymph node lesions. Based on this high classification precision, we believe the output activation map of the final layer of the ResNet-34 is a powerful tool for the accurate diagnosis of lymph node lesions of abdominal lymphadenopathy from CT images.

Keywords: Deep Convolutional Neural Networks (DCNN); Computed Tomography (CT); Abdominal Lymphadenopathy.

Lymphadenopathy is a condition with abnormal size and/or consistency of lymph nodes. Etiologies include infections, autoimmune diseases, malignancies, histiocytosis, storage diseases, benign hyperplasia, medications, and iatrogenic causes. A thorough history and physical examination are critical in establishing its diagnosis (1). It is classified into localized and generalized lymphadenopathy if its origin is unknown. Patients with localized lymphadenopathy should be evaluated for etiologies associated with the region involved according to lymphatic

drainage patterns. Patients with generalized lymphadenopathy, defined as the enlargement of more than two noncontiguous lymph node groups, often indicate underlying systemic disease (1,2). Abdominal lymph nodes drain the lower extremities, pelvis, and abdominal organs. Although mesenteric lymphadenopathy is not usually evident upon physical examination, abdominal pain, backache, increased urinary frequency, constipation, and intestinal obstruction secondary to intussusception are possible symptoms (1). Mesenteric adenitis, which is difficult to differentiate from appendicitis (3), is thought to be viral in etiology and is characterized by right lower quadrant abdominal pain caused by nodal enlargement near the ileocecal valve. Non-Hodgkin lymphoma, typhoid fever, and ulcerative colitis are also among mesenteric adenopathy's etiologies (3,4).

Lymphoma frequently results in lymphadenopathy in the chest, retroperitoneum, or superficial lymph node chains; however, mesenteric lymphadenopathy is not uncommon (5). Enlarged nodes may be seen at the mesenteric root, scattered throughout the peripheral mesentery, or mixed root-peripheral pattern (6). Early in the disease, the lymph nodes may be small and discrete; upon disease progression, the nodes often merge, forming a conglomerate soft-tissue mass. Lymphoma is a soft tissue tumor, and extensive mesenteric lymphadenopathy due to lymphoma has a characteristic appearance (7).

State-of-the-art Computed Tomography (CT) scanners currently offer excellent contrast and spatial resolution, often resulting in visualization of normal retroperitoneal and mesenteric lymph nodes (2). The sole criterion to determine if a lymph node is abnormal is enlarged size since CT cannot display abnormal architecture in a normal-sized node (8). This is the most significant shortcoming of the technique and a source of most false-negative results from CT examinations (7). Additional false-negative results are artifacts due to partial volume averaging and variable respiratory excursions. Radiologists interprets enhanced abdominal CT images and determine whether lymphatic metastasis has occurred based on the lymph nodes' texture, shape, size, and morphology (9). However, it often remains challenging for the radiologist to make correct and timely decisions by combining these features, especially for significant cases for which the accuracy of diagnosis certainly decreases, and errors are likely to occur (7,9). Therefore, it is necessary to develop more convenient, faster, and more accurate software or systems that can assist radiologists in quickly identifying peri-gastric metastatic lymph nodes. Artificial intelligence-assisted image recognition techniques are currently able to detect the target area of an image and make classifications according to target features, which is like the diagnosis process of the radiologist. We recently have shown that Deep Convolutional Neural Networks (DCNN) with transfer learning, which reuses parts of a previously trained model in a specific field for another task in a new model, could diagnose COVID-19 patients from chest X-ray images with very high precision (10). Moreover, DCNN has also been successfully used for computer-aided diagnosis of cervical lymph nodes in CT images using deep learning (11).

The objective of the present study was to employ the DCNN ResNet-34 for detecting and classifying lymph node lesions in CT images from patients with abdominal lymphadenopathy and healthy controls.

MATERIALS AND METHODS

Study Population Database and Sample Size

An expert radiologist determined the diagnosis of abdominal lymphadenopathy from CT images as the gold standard based on the location, shape, size, number, type, and extent of lymph node lesions due to infections, autoimmune diseases, malignancies, histiocytosis, storage diseases, benign hyperplasia, medications, and iatrogenic causes. We created a database containing a sample size of 1400 source CT images from online anonymous abdominal lymphadenopathy patients (n = 700) and healthy controls (n = 700), achieving a confidence level of 99% and a margin of error of 1% for the proposed DCNN model.

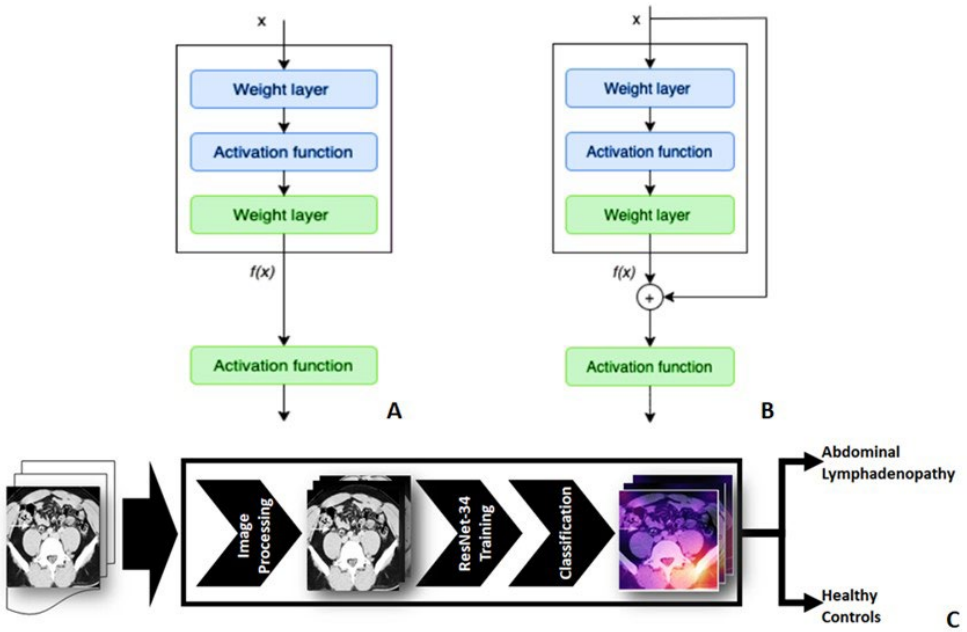

Fig. 1. *Block diagrams of a regular Convolutional Neural Network (CNN) (A), a residual Deep Convolutional Neural Network (DCNN) (B), and the arrangement of a three-step pipeline for the detection and classification of CT images using DCNN (C).*

The Ethics Committee of the Medical Research Institute, Alexandria University, approved the study protocol.

Deep Convolutional Neural Network Model Selection

Transfer learning is a supervised machine learning technique that uses less training data, better generalization, and affordable deep learning. Applying transfer learning to a pre-trained Residual Neural Network (ResNet) has proven useful for training a new DCNN for image recognition by modifying the activation function Softmax and the classification layer (10). We trained, validated, and tested the supervised pre-trained ResNet-34, a benchmarked DCNN model with an error rate as low as 3.6% (12), to classify the database of 1400 CT images. We employed the Adam optimization algorithm to train a multilayer feed-forward ResNet-34 model with backpropagation of errors, adjusting the learning rate to 10^{-3} and using a batch size of 16 random CT images (i.e., of patients with abdominal lymphadenopathy or healthy controls). The ResNet-34 structure has a moderate computational complexity, with 26.70 and 8.58 top-1 and top-5 errors, respectively (13). We finally evaluated the model using the PyTorch Library of the Anaconda Package (Anaconda Inc., New York, USA) under Mojave 10.14.6 running on a MacBook Pro (Intel i5-core @ 2.7 GHz processor and 16 GB RAM) (10).

We applied the Gradient-Weighted Class Activation Map (Grad-CAM) to localize and highlight a critical region of interest, identifying and labeling specific lymph node lesions with automatic volume delineation and 3D reconstruction of target areas for a particular category within an input CT image, as detailed elsewhere (10). Grad-CAM uses the gradient information of a target class flowing back into the last convolutional layer of the ResNet-34 for generating visual explanations in the form of class activation maps from the residual block (*Figs. 1A and 1B*), where it fed the global average pooled convolutional

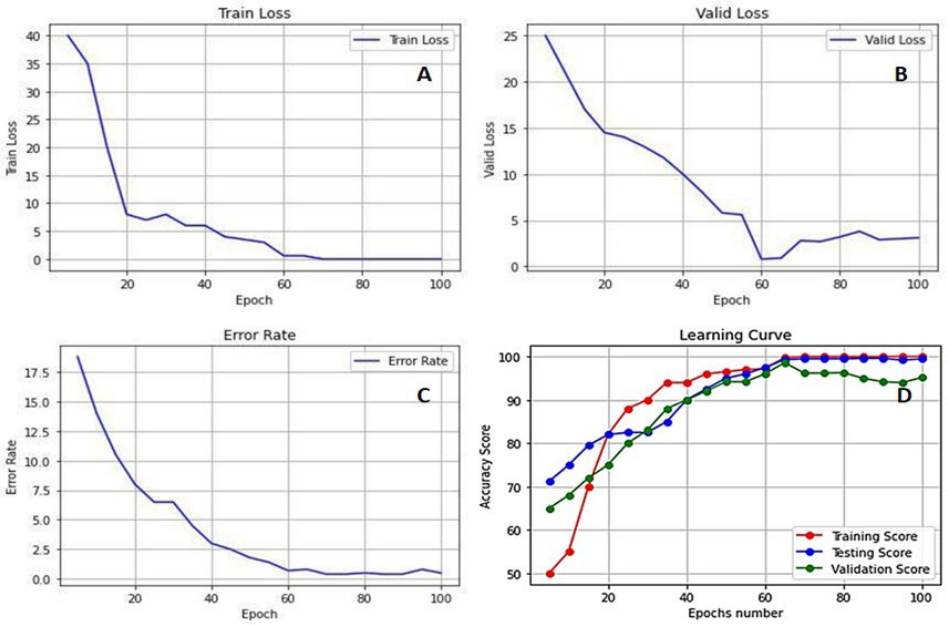

Fig. 2. Deep Convolutional Neural Network (DCNN) ResNet-34 performance as Training Loss (A), Validation Loss (B), Error Rate (C), and Accuracy Score of the three learning phases (i.e., Training, Testing, and Cross-Validation) (D) for patients with abdominal lymphadenopathy and healthy control CT images.

feature maps into the fully connected final output layer. The ResNet-34 block diagram for detection and classification is shown in *Figure 1C*, which consists of a three-step pipeline for: 1) detecting random CT images, where the first layers detect edges and shapes, while the last layers work on the details; 2) identifying all suspicious lesions in the abdominal CT image; and 3) classifying (i.e., diagnosing) of abdominal lymphadenopathy patients from healthy controls.

All CT images were resized to 224 × 224, normalized, and arranged in *m* groups of 16 images to match input requirements standards of the ResNet-34. The 1400 CT images were randomly divided into 88 groups of 16 images, where training was carried out using 53 groups (60%), validation using 18 groups (20%), and testing using the remaining 18 groups (20%). Passing CT image groups through the ResNet-34 for training, group normalization between skips double- or triple-layers containing non-linearities for image classification (14). The performance of the ResNet-34 was monitored as the training loss, validation loss, and error rate along with epochs, each epoch represents a full iteration of the training dataset. The classification accuracy was assessed by the receiver operating characteristic (ROC) curve, the area under the curve (AUC), sensitivity and specificity analysis, and the confusion matrix for actual versus predicted values of abdominal lymphadenopathy and healthy control CT images. Finally, K-Fold cross-validation tests were carried out for classifying all source CT images from abdominal lymphadenopathy patients and healthy controls, divided equally randomly among each one-to-five-fold, respectively.

RESULTS

Figures 2A to 2C show the performance of the ResNet-34 model, where the training and validation loss of random subsets of CT images and the error rate with the number of

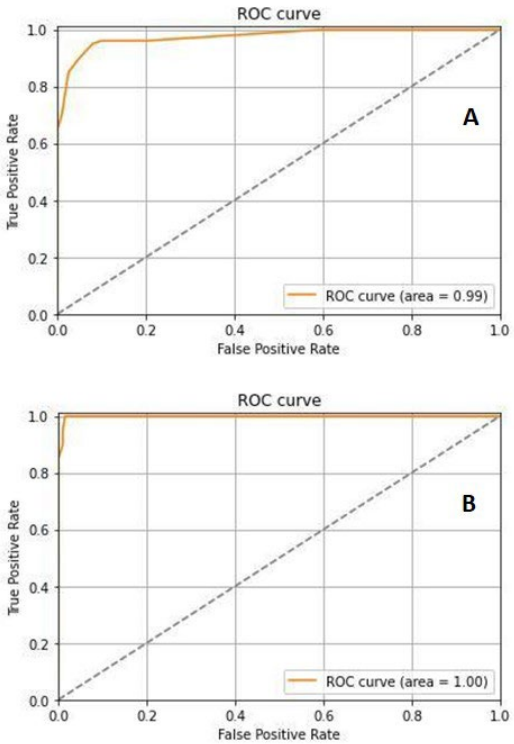

Fig. 3. *The receiver operating characteristic (ROC) curve analysis of sensitivity against 1 – specificity for patients with abdominal lymphadenopathy (A) and healthy control (B) CT images.*

TABLE 1
Accuracy and Error Rate of K-Fold Cross-Validation Tests

K-Fold	Accuracy (%)	Error Rate
1	99.39	6.08×10^{-3}
2	99.45	5.42×10^{-3}
3	99.57	5.39×10^{-3}
4	98.34	6.58×10^{-3}
5	98.86	1.14×10^{-2}
Average Result	***99.30***	***6.97×10^{-3}***

epochs converge at the end of the training phase. Sixty-two epochs were sufficient to avoid under- and over-fitting, reflecting the high precision of testing the subset of random CT images used to detect and classify lymph node lesions. *Figure 2D* shows that the accuracy score of the training, testing, and validation phases attained maximum values beginning at epoch 62.

Fundamental measures of the diagnostic accuracy of the ResNet-34 model, as of ROC curves of the true-positive rate versus the false positive rate, for patients with abdominal lymphadenopathy and healthy control CT images are shown in *Figures 3A and 3B*. AUC values for patients with abdominal lymphadenopathy and healthy controls were 0.9957 and 1.00, which signify a perfect accuracy in the diagnosis and identical sensitivity and specificity values of 99.57% and 100% for the two groups, respectively, with an error rate of 5.39×10^{-3} by three-fold cross-validation test, as shown in *Table 1*. The ResNet-34 achieved a high average accuracy of 99.30% and a low error rate of 6.97 10^{-3} in classifying all source CT images.

Moreover, the confusion matrix (*Fig. 4)* shows that the ResNet-34 had a success rate of 99.57 and 100% for classifying all source CT images of patients with abdominal lymphadenopathy and healthy controls, respectively. The overall accuracy of the ResNet-34 for testing the subset of random CT images was as high as 99.79%, which means an error rate as

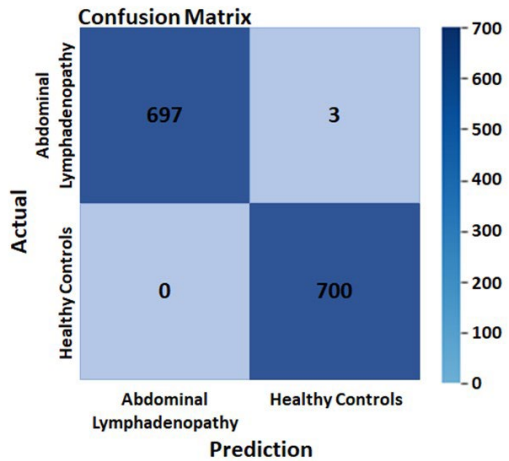

Fig. 4. *Confusion matrix of detection and classification results for patients with abdominal lymphadenopathy and healthy control CT images.*

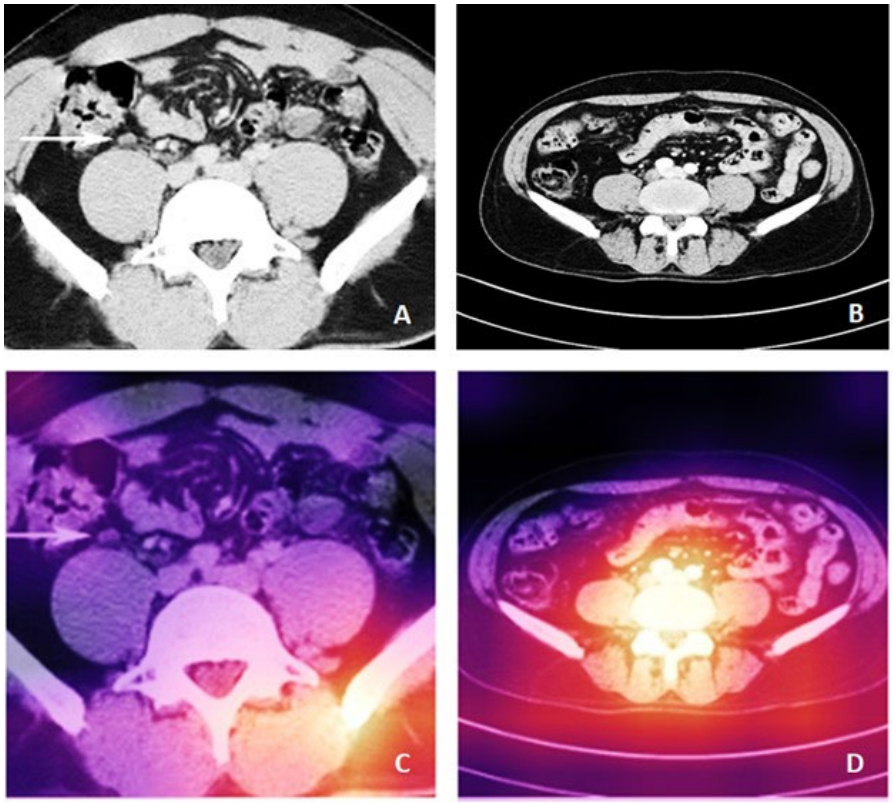

Fig. 5. *Example of input grayscale CT images for a patient with abdominal lymphadenopathy (A) and a healthy control (B). Output colored activation maps of the same CT images for a patient with abdominal lymphadenopathy (C) and a healthy control (D).*

low as 0.21%. Figures 5A and 5B show samples of input CT grayscale images batch for patients with abdominal lymphadenopathy and healthy controls. Figures 5C and 5D also show samples of the colored activation map of the ResNet-34 final output layer for the two different subsets. The activation map is a proper visual diagnostic representation, highlighting specific lymph node lesions of a CT image contributing to the added effect of the ResNet-34 classification process.

DISCUSSION

Lymphadenopathy is a broad term describing lymph node pathology that does not necessarily result in increased size but rather includes their atypical number and derangement of internal architecture. Sarcoidosis, tuberculosis, mastocytosis, Crohn's disease, Whipple disease, and nontropical sprue may cause lymph node enlargement. However, an increase in lymph node size is not always pathologic since some nodes are bigger than others normally due to a healthy reactive response. It has been shown that 5%-10% of CT detected abdominal lymphadenopathy cases are related to benign processes rather than malignant infiltration. Unfortunately, there are no distinctive features distinguishing benign from malignant lymphadenopathy since individual nodes greater than 2 cm and confluent node mantles may be seen in benign diseases (9).

Computer-aided diagnosis (CAD) has proven important in medical imaging and diagnostic radiology, helping radiologists acquire, manage, store, and report medical images from various imaging techniques (e.g.,

CT, MRI, US, and CR) (15,16). More precisely, CAD is a pattern recognition software that identifies suspicious features on an image in clinical practice that aids radiologists in detecting potential abnormalities on diagnostic radiology exams. Our proposed CAD system based on the ResNet-34 model showed a very high performance due to the convergence of the training loss, validation loss, and error rate to a minimum (i.e., zero) (*Figs. 2A to 2C*). The ResNet-34 builds on constructs from pyramidal cells in the cerebral cortex using skip connections or shortcuts to jump over some layers, which permits the advantageous reduction of over-fitting and leads to faster optimization and better performance of the DCNN model. Only 62 epochs were sufficient to attain a high and stable accuracy score of training, testing, and cross-validation of random CT images without under- or over-fitting (*Fig. 2D*).

Moreover, AUC analysis of ROC curves (*Figs. 3A and 3B*) of true-positive rate (i.e., sensitivity) versus false-positive rate (i.e., 1–specificity) showed that points in the upper left corner signify sensitivity and specificity as high as 99% and 100% for abdominal lymphadenopathy and healthy controls, respectively, by three-fold cross-validation test (*Table 1*). These results outperform those by Liu *et al.* (17), who proposed a CAD system based on a 3D blob enhancement filter for the automatic detection of enlarged lymph nodes in contrast-enhanced abdominal CT images from 9 patients compared to the original multi-scale Hessian analysis performance. Their method achieved a sensitivity and false-positive rate of 91% and 17% compared to 82% and 28% for the multi-scale Hessian analysis. Bejnordi *et al.* (18), have evaluated the performance of automated DCNN algorithms for detecting metastases in hematoxylin and eosin-stained tissue sections of lymph nodes from women with breast cancer compared to pathologists' diagnoses. They have shown that some DCNN algorithms achieved better diagnostic performance than a panel of the 11 pathologists who participated in the simulation exercise designed to mimic routine pathology workflow. The top-performing algorithm achieved a lesion-level, true-positive fraction comparable with that of the pathologist without time constraints of 72.4% at a mean of 0.0125 false positives per normal whole-slide image. The AUC of the best algorithm for the whole-slide image classification task was 0.994, which performed significantly better than the pathologists (0.810, $p < 0.001$) with time constraints in a diagnostic simulation. Moreover, the performance of the top 5 algorithms was comparable with an expert pathologist (AUC: 0.960 vs. 0.966) interpreting whole-slide images without time constraints, yet their approach was not evaluated in a clinical setting.

The added effect due to the success rate of the ResNet-34 was 99.57% and 100% for classifying all source CT images of abdominal lymphadenopathy and healthy controls, respectively (*Fig. 4*). The overall accuracy of the ResNet-34 for testing the subset of random CT images used for the detection and classification of lymph node lesions was as high as 99.79%, with a very low error rate of 0.21% in the testing phase compared to the 3.6% showed for the benchmarked ResNet-34 (12). We have recently shown similar results using the same ResNet-34 model, which showed high-performance and precision in detecting and classifying COVID-19, pneumonia, and the normal controls from CXR images with an accuracy of 100%, 99.6%, and 98.9, with an overall accuracy of 99.5% for the testing subset for diagnosis (10).

It has been shown that 5%-10% of CT detected abdominal lymphadenopathy cases are related to benign processes rather than malignant infiltration. Unfortunately, there are no distinctive features distinguishing benign from malignant lymphadenopathy since individual nodes greater than 2 cm and confluent node mantles may be seen in benign diseases (9). We employed the Grad-CAM method to localize and visualize an ROI within CT images, consistently highlighting a specific area common in shape, pattern, or location among CT images within the same class but distinct from images in other modality classes (14). The activation map (*Figs. 5C and 5D*) is thus an informative visual diagnostic representation, highlighting certain mor-

phological anomalies of lymph nodes in a CT image contributing the most to the ResNet-34 classification process.

Rahman *et al.* (19), have recently addressed the problem of automatically classifying gastrointestinal polyps using a stacking ensemble technique consisting of three fine-tuned DCNN architectures; Xception, ResNet-101, and VGG-19; where the network weights were initialized from the ImageNet dataset. They applied a set of endoscopic image enhancement operations to remove specular reflection, clipping unnecessary regions, contrast enhancement, and noise reductions. Using five-fold cross-validation, they attained an accuracy of 98.53%, a recall score of 96.17%, a precision value of 92.09%, a specificity score of 98.97%, and an AUC score of 0.99. Thus, the specified polyps' classification method showed significantly improved performance metrics on available public datasets, which could be helpful for endoscopists to make accurate decisions.

The DenseNet-169 CNN model has been employed successfully to analyze digitized slides of prophylactic gastrectomy specimens from seven patients with germline CDH1 mutations to detect 133 carcinoma foci, which achieved an AUC of 0.9986 on individual patches and 0.9984 on the external validation dataset (20). The model had a sensitivity of 90% with a false-positive rate of less than 0.1%. The network detected 100% of carcinoma foci on whole slide images, correctly eliminating an average of 99.9% of the non-cancer slide area from consideration.

Moreover, Liu *et al.* (21), have successfully employed a 3D U-Net model for the automatic detection and segmentation of lymph nodes on 393 pelvic diffusion-weighted imaging images for patients suspected of prostate cancer. The dice score, true positive rate, positive predictive value, volumetric similarity, Hausdorff distance, average distance, and Mahalanobis distance values for the segmentation of suspicious lymph nodes were 0.85, 0.82, 0.80, 0.86, 2.02 (mm), 2.01 (mm), and 1.54 (mm) respectively. The precision, recall, and F1-score for detecting suspicious lymph nodes were 0.97, 0.98, and 0.97, respectively. In the temporal validation dataset, the AUC of the model for identifying prostate cancer patients with suspicious lymph nodes was 0.96, with a high consistency of lymph node staging for the model and an expert radiologist (k = 0.92).

Iuga *et al.* (22), have also recently developed an automatic tool for the 3D detection and segmentation of lymph nodes in 89 contrast-enhanced CT scans of the thorax using a DCNN U-Net based on 3D foveal patches. The algorithm achieved good overall performance with a total detection rate of 76.9% for enlarged lymph nodes during fourfold cross-validation in the training dataset with 10.3 false positives per volume and 69.9% in the unseen testing dataset. A better detection rate was observed in the training dataset for enlarged than smaller lymph nodes; the detection rates for lymph nodes with a short-axis diameter ≥ 2 cm and 0.5-1 cm were 91.6% and 62.2% ($p < 0.001$), respectively. Best detection rates for lymph nodes located in Level 4R and Level 7 were 83.6% and 80.4%, respectively.

CONCLUSIONS

A highly expert radiologist is required for diagnosing morphological anomalies of lymph node lesions in CT images. We employed the ResNet-34 to detect and classify CT images of patients with abdominal lymphadenopathy and healthy controls. Images were resized, normalized, without any image augmentation, and arranged in *m* groups of 16 images before supervised training and validation of the DCNN classifier. The added effect of the ResNet-34 model is a success rate of 99.57% and 100% for classifying random CT images of patients with abdominal lymphadenopathy and healthy controls, with an overall accuracy of 99.79% in the testing subset for detecting and classifying lymph node lesions. Based on this high classification precision, we believe the output activation map of the final layer of the ResNet-34 is a powerful tool for the accurate diagnosis of abdominal lymphadenopathy from CT images.

ACKNOWLEDGMENTS

The authors would like to thank Dr. Atef K. Khamis for professional assistance in preparing the CT images database for Abdominal Lymphadenopathy patients and Healthy Control.

CONFLICT OF INTEREST AND DISCLOSURE

All authors declare no financial, commercial, legal, or professional relationship with other organizations or the people working with them that could influence the research results.

SOURCES OF SUPPORT

All authors declare not receiving any financial support for conducting this research.

REFERENCES

1. Gaddey, HL, AM Riegel: Unexplained lymphadenopathy: Evaluation and differential diagnosis. Am. Fam. Physician 94 (2016), 896-903.
2. Maini, R, S Nagalli: Lymphadenopathy. In: StatPearls [Internet]. StatPearls Publishing, Treasure Island, 2022.
3. Alvarado, A, DV Garbuzenko (Ed): Clinical approach in the diagnosis of acute appendicitis. In: Current Issues in the Diagnostics and Treatment of Acute Appendicitis. Intech Open, London, 2018.
4. Spijkers, S, JM Staats, AS Littooij, et al: Abdominal lymph node size in children at computed tomography. Pediatr. Radiol. 50 (2020), 1263-1270.
5. Yu, RS, WM Zhang, YQ Liu: CT diagnosis of 52 patients with lymphoma in abdominal lymph nodes. World J. Gastroentero. 12 (2006), 7869-7873.
6. Helbling, R, E Conficconi, M Wyttenbach, et al: Acute nonspecific mesenteric lymphadenitis: More than "No Need for Surgery." Biomed. Res. Int. (2017), 9784565.
7. Lucey, BC, JW Stuhlfaut, JA Soto: Mesenteric lymph nodes seen at imaging: Causes and significance. Radiographics 25 (2005), 351-365.
8. Witte, CL, MH Witte, EC Unger, et al: Advances in imaging of lymph flow disorders. Radiographics 20 (2000), 1697-1719.
9. Einstein, DM, AA Singer, WA Chilcote, et al: Abdominal lymphadenopathy: Spectrum of CT findings. Radiographics 11 (1991), 457-472.
10. Salama, AA, SH Darwish, SM Abdel-Mageed, et al: Deep convolutional neural networks for accurate diagnosis of COVID-19 patients using chest X-ray image databases from Italy, Canada, and the USA. Univ. Louisville J. Resp. Infect. 5 (2021), 34.
11. Tekchandani, H, S Verma, ND Londhe, et al: Computer aided diagnosis system for cervical lymph nodes in CT images using deep learning. Biomedical Signal Processing and Control. 71 (2022), 103158.
12. Koustubh: ResNet, AlexNet, VGGNet, inception: Understanding various architectures of Convolutional Networks. CV-Tricks.com: Learn Machine Learning, AI & Computer Vision. Accessed February 26, 2021.
13. Paszke, A, S Gross, F Massa, et al: In: Wallach H, Larochelle H, Beygelzimer A, d'Alché-Buc F, Fox E, Garnett R (Eds.), Advances in Neural Information Processing Systems 32, Curran Associates, Inc. (2019), 8024-8035.
14. Kim, I, S Rajaraman, S Antani.: Visual interpretation of convolutional neural network predictions in classifying medical image modalities. Diagnostics 9 (2019), 38.
15. Castellino, RA: Computer aided detection (CAD): An overview. Cancer Imaging 5 (2005), 17-19.
16. Doi, K: Computer-aided diagnosis in medical imaging: Historical review, current status and future potential. Comput. Med. Imaging Grap. 31 (2007), 198-211.
17. Liu, JM, J Hua, JH Yao, et al: Computer-aided abdominal lymph node detection using contrast-enhanced CT images. Proceedings of SPIE 7963 (2011), 796313.
18. Bejnordi, BE, M Veta, PJV Diest, et al: Diagnostic assessment of deep learning algorithms for detection of lymph node metastases in women with breast cancer. JAMA. 318 (2017), 2199-2210.
19. Rahman, MM. AH Wadud, M Hasan: Computerized classification of gastrointestinal polyps using stacking ensemble of convolutional neural network. Informatics in Medicine Unlocked 24 (2021), 100603.
20. Rasmussen, SA, T Arnason, WY Huang: Deep learning for computer-assisted diagnosis of hereditary diffuse gastric cancer. J. Pathol. Transl. Med. 55 (2021), 118-124.

21. Liu, X, Z Sun, C Han, et al: Development and validation of the 3D U-Net algorithm for segmentation of pelvic lymph nodes on diffusion-weighted images. BMC Med. Imaging 21 (2021), 170.
22. Iuga, AI, H Carolus, AJ Höink, et al: Automated detection and segmentation of thoracic lymph nodes from CT using 3D foveal fully convolutional neural networks. BMC Med. Imaging. 21 (2021), 69.

Prof. Ehab I. Mohamed
Head, Department of Medical Biophysics
Medical Research Institute; University of Alexandria
165 El-Horreya Avenue; 21561 Alexandria, Egypt
Voice: +20 (0)3 428 2331/ 2373/ 3543/ 5455
Fax: +20 (0)3 428 3719
Mobile:+20 (0)122 932 2010
Email: eimohamed@yahoo.com; ehab.abdo@alexu.edu.eg